Research Square

Preprints are preliminary reports that have not undergone peer review. They should not be considered conclusive, used to inform clinical practice, or referenced by the media as validated information.

Green-Synthesised Silver Nanoparticles from Solanum aethiopicum Leaves: Physicochemical Characterisation and In Vitro Antioxidant Activity

Chinwe P. Okonkwo
Nnamdi Azikiwe University

Matthew C. Obiadi
Nnamdi Azikiwe University

Anthony A. Anyogu
Nnamdi Azikiwe University

Julie O. Ndubuisi
Federal University of Allied Health Sciences, Enugu

Benjamin C. Asogwa
University of Nigeria

Jude I. Ayogu
jude.ayogu@unn.edu.ng

University of Nigeria

Research Article

Keywords: silver nanoparticles, Solanum aethiopicum, green synthesis, antioxidant activity, oxidative stress, lipid peroxidation, phytochemical capping, nanomedicine

Posted Date: August 4th, 2026

DOI: https://doi.org/10.21203/rs.3.rs-10538856/v1

License: This work is licensed under a Creative Commons Attribution 4.0 International License. Read Full License

Additional Declarations: No competing interests reported.

Abstract

Green synthesis of silver nanoparticles (AgNPs) using medicinal plants provides a sustainable route for producing bioactive nanomaterials. In this study, aqueous leaf extract of *Solanum aethiopicum* was employed as a reducing and capping agent for the biosynthesis of AgNPs, which were subsequently characterised and evaluated for their *in vitro* antioxidant activity. Nanoparticle formation was confirmed by a visible colour change and a characteristic surface plasmon resonance band at approximately 420 nm. FTIR analysis indicated the involvement of hydroxyl, carbonyl, amine, aromatic and ether-containing phytochemicals in nanoparticle reduction and stabilisation. TEM showed predominantly spherical nanoparticles with representative diameters of approximately 9.22 and 12.54 nm, while XRD confirmed crystalline face-centred cubic silver with an average crystallite size of approximately 16.5 nm. The biosynthesised AgNPs inhibited malondialdehyde formation by 94.48–96.07%, with calculated inhibition values numerically higher than those obtained for ascorbic acid under the same assay conditions. The available biochemical data also showed concentration-associated SOD and CAT assay responses, with the highest values observed at 6 mg mL^{-1}, together with a concentration-associated increase in GSH response across the tested concentrations. Because replicate-level data were unavailable, these findings were interpreted descriptively rather than as statistically confirmed treatment effects. Collectively, the findings show that *S. aethiopicum*-derived AgNPs are phytochemically capped, crystalline nanostructures that markedly inhibited lipid peroxidation and produced concentration-associated SOD, CAT and GSH assay responses under the experimental conditions. These results support further investigation in cellular, toxicological and in vivo models relevant to oxidative stress.

1. Introduction

Cancer remains one of the leading causes of morbidity and mortality worldwide and continues to impose a major burden on public health despite substantial advances in diagnosis and treatment.[1] Recent global estimates show that cancer accounts for millions of new cases and deaths each year, and the burden is expected to rise further because of population growth, ageing, and changing environmental and lifestyle-related risk factors.[2–4] Although surgery, chemotherapy, radiotherapy, targeted therapy, and immunotherapy have improved outcomes in many settings, their clinical usefulness is often limited by severe adverse effects, poor tumour selectivity, multidrug resistance, recurrence, and high cost.[1] These limitations continue to drive the search for safer and more effective therapeutic strategies.

A growing body of evidence indicates that oxidative stress plays a central role in the pathogenesis of cancer and many other chronic diseases, including cardiovascular disorders, diabetes mellitus, neurodegenerative diseases, and inflammatory conditions.[5–7] Oxidative stress arises when the production of reactive oxygen species (ROS) exceeds the capacity of endogenous antioxidant systems to maintain redox homeostasis. While ROS are naturally generated during normal cellular metabolism and also function as important signalling molecules, excessive ROS accumulation can damage lipids, proteins, carbohydrates, and nucleic acids, thereby promoting genomic instability, mitochondrial

dysfunction, altered signal transduction, and dysregulated cell proliferation.[6–8] In cancer biology, this relationship is especially important because tumour cells frequently maintain elevated ROS levels that can support proliferation, angiogenesis, invasion, and metastatic progression, while excessive oxidative burden may also push cells toward apoptosis. This dual role has made redox modulation an important area of interest in biomedical research.

Nanotechnology has emerged as a promising platform for addressing such challenges through the development of materials with dimensions typically in the range of 1-100 nm and physicochemical properties distinct from those of their bulk counterparts. [9, 10] Because of their small size, high surface-area-to-volume ratio, tunable surface chemistry, and unique optical, catalytic, and electronic properties, nanomaterials have found increasing application in drug delivery, biosensing, imaging, tissue engineering, antimicrobial therapy, and cancer research. Within this broad field, silver nanoparticles (AgNPs) have attracted considerable attention owing to their broad-spectrum biological activities, including antimicrobial, anti-inflammatory, antioxidant, and cytotoxic effects in different biological contexts.[11–13] Their biological behaviour is strongly influenced by key physicochemical parameters such as particle size, morphology, crystallinity, aggregation state, and surface functionalisation, all of which may affect their interaction with biomolecules and cellular redox systems.

The method of nanoparticle synthesis is particularly important because it directly shapes the structural and biological properties of the final material. Conventional physical and chemical synthesis methods often involve high energy input, expensive instrumentation, and hazardous reducing or stabilising agents that may generate toxic residues and reduce suitability for biomedical use.[14–16] In contrast, green synthesis has emerged as a more sustainable and biologically attractive alternative. Plant-mediated synthesis is especially appealing because it is simple, relatively low-cost, and environmentally compatible, while avoiding the use of harsh synthetic chemicals. Plant extracts contain a wide range of phytochemicals, including flavonoids, phenolic acids, tannins, alkaloids, terpenoids, proteins, and reducing sugars, which can act simultaneously as reducing agents and stabilising or capping molecules during nanoparticle formation.[11, 15, 16] This phytochemical-mediated capping is particularly relevant because it may improve nanoparticle stability and influence subsequent biological activity, including antioxidant behaviour.

Among plant resources with potential for green nanotechnology, *Solanum aethiopicum* L. is of particular interest. Commonly known as African eggplant or garden egg, it is an important indigenous vegetable widely cultivated and consumed across sub-Saharan Africa.[17] Beyond its nutritional value, *S. aethiopicum* has recognised ethnomedicinal importance and has been traditionally associated with the management of inflammatory and other health-related conditions. Phytochemical investigations have shown that its leaves and fruits contain biologically active constituents such as flavonoids, phenolic compounds, alkaloids, tannins, saponins, and terpenoids, many of which are associated with antioxidant and protective effects. [11] These metabolites make the plant a plausible candidate for the green synthesis of

AgNPs, where the same compounds may contribute both to silver ion reduction and to stabilisation of the resulting nanostructures.

Recent studies on plant-derived AgNPs have shown that the biological properties of these nanomaterials often depend not only on the silver core itself but also on the surrounding phytochemical corona.[12] In antioxidant systems, biosynthesised AgNPs have been reported to suppress lipid peroxidation, scavenge reactive oxygen species, and modulate endogenous antioxidant defence systems, including superoxide dismutase (SOD), catalase (CAT), and reduced glutathione (GSH).[12] In addition to these antioxidant effects, plant-mediated silver nanoparticles have been investigated for their potential relevance in cancer research through redox-mediated mechanisms involving reactive oxygen species modulation, mitochondrial dysfunction, and apoptosis induction.[18] However, these biological responses are strongly influenced by nanoparticle dose, particle size, surface chemistry, and the experimental model employed.[18, 19] For that reason, careful distinction is necessary between demonstrated antioxidant findings and broader biomedical implications. In the present work, the available thesis data support green synthesis, physicochemical characterisation, and in vitro antioxidant assessment but do not provide direct cancer cell-based evidence such as cytotoxicity, apoptosis, or intracellular ROS assays. Accordingly, any implication for anticancer application should be regarded as prospective rather than demonstrated.

Despite increasing interest in plant-mediated silver nanoparticle synthesis, [11, 15] studies focusing specifically on *Solanum aethiopicum* leaves remain limited, and the relationship between nanoparticle characteristics and antioxidant performance is not yet well established. This gap is important, particularly in the context of developing sustainable nanomaterials from locally available medicinal plants. A systematic evaluation of *S. aethiopicum*-mediated AgNPs may therefore provide useful baseline information on nanoparticle formation, phytochemical participation, structural features, and redox-related bioactivity.

Therefore, the present study aimed to synthesise silver nanoparticles using aqueous leaf extract of *Solanum aethiopicum* through a green route, characterise the resulting nanoparticles using ultraviolet-visible spectroscopy (UV-Vis), Fourier-transform infrared spectroscopy (FTIR), transmission electron microscopy (TEM), and X-ray diffraction (XRD), and evaluate their in vitro antioxidant activity using malondialdehyde (MDA), superoxide dismutase (SOD), catalase (CAT), and reduced glutathione (GSH) assays. By integrating plant-based synthesis, physicochemical characterisation, and biochemical antioxidant evaluation, this study provides a more accurate foundation for understanding the bioactivity of *S. aethiopicum*-derived AgNPs and their prospective relevance in oxidative stress-related biomedical research.

2. Materials and Methods

2.1 Materials

Silver nitrate ($AgNO_3$, ≥ 99%, UNICON), thiobarbituric acid (TBA, 99%, SRL), trichloroacetic acid, potassium dichromate ($K_2Cr_2O_7$), glacial acetic acid, phosphate buffer, ferric chloride ($FeCl_3$, anhydrous, 98%, SRL), ascorbic acid, epinephrine, hydrogen peroxide and all other reagents were of analytical grade and used as received. Distilled water was used throughout the experiments.

Nanoparticle synthesis and characterisation were performed using a UV–Vis spectrophotometer (752P, Searchtech Instrument, UK), orbital shaker (YR06065, Kalstein), centrifuge (Model 800B, Searchtech Instrument, UK), incubator (DNP-9022-1A, Gulfex Medical and Scientific), water bath (HH-W420, Searchtech Instrument, UK), laboratory oven (Heraeus B5050 F), and analytical balance (Mettler Toledo, USA). Standard borosilicate laboratory glassware and consumables were used throughout the study.

2.2 Collection and Preparation of Plant Material

Fresh leaves of *Solanum aethiopicum* were collected from Awka, Anambra State, Nigeria, and authenticated at the Department of Botany, Nnamdi Azikiwe University, Awka. The leaves were thoroughly washed with distilled water to remove adhering dust and debris and then air-dried at room temperature for two weeks. The dried leaves were cut into smaller pieces and stored in clean containers until use.

For extraction, 100 g of the dried leaf material was boiled in 1 L of distilled water at 80°C for 20 min. The mixture was allowed to cool and subsequently filtered using Whatman No. 1 filter paper. The resulting filtrate was collected and stored at 4°C for further use in nanoparticle synthesis.

2.3 Biosynthesis of Silver Nanoparticles

A 2 mM aqueous silver nitrate solution was prepared using distilled water. Thereafter, 200 mL of the *S. aethiopicum* leaf extract was added dropwise to 1000 mL of the silver nitrate solution under continuous stirring at room temperature for 30 min. Nanoparticle formation was initially indicated by a visible change in the reaction mixture from dark green to light brown, with subsequent development of a darker brown colour. The resulting suspension was then centrifuged at 4000 rpm for 20 min. The recovered pellet was washed repeatedly with distilled water to remove residual impurities and unreacted constituents. The purified nanoparticles were dried in an oven at 60°C, powdered and stored at 4°C until characterisation and biological evaluation.

2.4 Physicochemical Characterisation of Biosynthesised AgNPs

2.4.1 UV–Visible Spectroscopy

The formation of silver nanoparticles was monitored using UV–Visible spectroscopy as described for plant-mediated AgNP synthesis. Aliquots of the reaction mixture were analysed using a UV–Visible spectrophotometer (752P, Searchtech Instrument, UK) over a wavelength range of 300–700 nm against

distilled water as the blank. Absorption maxima corresponding to the surface plasmon resonance (SPR) band of silver nanoparticles were recorded.

2.4.2 Fourier Transform Infrared Spectroscopy

Fourier-transform infrared spectroscopy was performed to identify functional groups associated with the biosynthesised AgNPs. Dried nanoparticle samples were prepared using the KBr pellet technique at a sample-to-KBr ratio of 1:100. Spectra were recorded over the range 4000–400 cm^{-1} at a resolution of 4 cm^{-1} using 32 scans and the principal absorption bands were assigned according to characteristic vibrational frequencies.

2.4.3 Transmission Electron Microscopy

The morphology and representative particle dimensions of the biosynthesised AgNPs were examined using transmission electron microscopy (TEM). A drop of diluted nanoparticle suspension was deposited onto a carbon-coated copper grid and allowed to air-dry before imaging. Representative TEM micrographs were used to assess nanoparticle morphology, approximate particle dimensions and visible agglomeration. The TEM observations were interpreted qualitatively and were not used to derive a statistically based particle-size distribution.

2.4.4 X-ray Diffraction Analysis

The crystalline structure of the biosynthesised silver nanoparticles was examined by X-ray diffraction (XRD) using a PANalytical X'Pert PRO diffractometer (PANalytical B.V., Netherlands). The dried nanoparticle sample was pelletised, sieved to a particle size of approximately 0.01 mm and placed in an aluminium-alloy sample holder. Diffraction measurements were performed at room temperature using Cu Kα radiation ($\lambda = 1.5406$ Å; 0.15406 nm), with the instrument operated at 40 kV and 30 mA and a scanning rate of 2° min^{-1}. The resulting diffraction data were compared with the standard powder-diffraction pattern for face-centred cubic metallic silver.

The average crystallite size was estimated from the broadening of the principal diffraction peaks using the Debye–Scherrer equation:[20]

$$D = \frac{K\lambda}{\beta \cos\theta}$$

where D is the mean crystallite size, K is the Scherrer shape factor, taken as 0.9 for approximately spherical particles, λ is the X-ray wavelength, β is the full width at half maximum (FWHM) of the diffraction peak expressed in radians, and θ is the corresponding Bragg angle.

2.5 Preparation of Tissue Homogenate for Biochemical Assays

Rat liver tissue was homogenised in cold phosphate buffer to obtain a 10% homogenate, followed by centrifugation to isolate the supernatant used for biochemical assays. Liver homogenate-based

oxidative stress models are commonly applied to assess the capacity of bioactive agents to suppress lipid peroxidation and influence antioxidant defence enzymes under controlled in vitro conditions.

2.6 *In-vitro* Antioxidant Assays

2.6.1 Malondialdehyde (MDA) assay (index of lipid peroxidation)

Lipid-peroxidation inhibitory activity was evaluated using the thiobarbituric acid-reactive substances (TBARS) assay, based on the methods of Ohkawa *et al.*,[21] and Buege and Aust (1978),[22] with minor modifications. The assay is based on the reaction of malondialdehyde and other thiobarbituric acid-reactive products formed during lipid peroxidation with thiobarbituric acid under acidic, high-temperature conditions to produce a pink-coloured complex measurable at 532 nm.

Rat liver tissue was homogenised in ice-cold phosphate buffer (0.1 M, pH 7.4) at a tissue-to-buffer ratio of 1:10 (w/v) to prepare a 10% liver homogenate. The homogenate was centrifuged at 3500 rpm for 10 min, and the resulting supernatant was collected for the assay.

The reaction mixture contained 0.5 mL of liver-homogenate supernatant, 0.5 mL of the test sample, buffer or control, and 0.1 mL of 0.1 mM $FeCl_3$. Phosphate buffer (1.1 mL) was added to bring the final reaction volume to 2.0 mL, after which the mixture was incubated at 37°C for 1 h to induce lipid peroxidation.

Following incubation, 1.0 mL of 15% trichloroacetic acid and 1.0 mL of 0.67% thiobarbituric acid were added. The mixture was vortexed, heated in a water bath at 95°C for 15–20 min, cooled and centrifuged at 3500 rpm for 10 min. The absorbance of the resulting supernatant was measured at 532 nm.

Ascorbic acid was used as the positive antioxidant control. The negative control contained phosphate buffer only (no pro-oxidant), while sample blanks containing all reagents except liver homogenate were included to correct for background absorbance attributable to the test samples. The AgNPs and ascorbic acid were evaluated at 2, 4 and 6 mg mL^{-1}.

Lipid-peroxidation inhibition was calculated as:

$\mathrm{Inhibition}(\%) = \left[1 - \frac{A_{\mathrm{sample}}}{A_{\mathrm{control}}}\right] \times 100$ where A_{sample} is the blank-corrected absorbance of the reaction containing the test sample and A_{control} is the absorbance of the control without the test compound.

2.6.2 Superoxide Dismutase (SOD) Activity Assay

Superoxide dismutase (SOD) activity was determined based on the inhibition of epinephrine auto-oxidation at alkaline pH according to the method of Sun and Zigman (1978), with minor modifications[23].

The assay is based on the ability of SOD to inhibit the oxidation of epinephrine to adrenochrome, the formation of which was monitored spectrophotometrically at 480 nm.

Briefly, the reaction mixture (3.00 mL) consisted of 2.95 mL of 0.05 M sodium carbonate buffer (pH 10.2), 0.02 mL of sample, and 0.03 mL of 0.30 mM epinephrine prepared in 0.005 N HCl, which was added to initiate the reaction. A reference cuvette containing 2.95 mL of carbonate buffer, 0.03 mL of epinephrine solution, and 0.02 mL of distilled water was used as the blank. The increase in absorbance resulting from adrenochrome formation was monitored at 480 nm for 3 min. SOD activity was calculated from the change in absorbance at 480 nm using the original experimental calculation, which applied the molar extinction coefficient of adrenochrome ($\varepsilon = 4020\ M^{-1}\ cm^{-1}$). The resulting values were expressed as U mL^{-1}.

2.6.3 Catalase (CAT) Activity Assay

Catalase (CAT) activity was determined according to the method of Sinha (1972)[24]. The assay is based on the decomposition of hydrogen peroxide by catalase, after which the residual hydrogen peroxide reacts with potassium dichromate in acetic acid upon heating to produce a chromic acetate complex measurable at 620 nm.

Briefly, the reaction mixture (1.50 mL) consisted of 1.00 mL of 0.01 M phosphate buffer (pH 7.0), 0.10 mL of sample and 0.40 mL of 2.0 M hydrogen peroxide. Following incubation at room temperature for 3 min, the reaction was terminated by the addition of 2.00 mL of dichromate–acetic acid reagent prepared by mixing 5% (w/v) potassium dichromate and glacial acetic acid in a 1:3 ratio. The reaction mixture was subsequently heated in a boiling water bath to allow colour development, cooled to room temperature, and the absorbance was measured at 620 nm using a UV–Visible spectrophotometer. Catalase activity was calculated according to the procedure described by Sinha (1972)[24] and expressed as U mL^{-1}.

2.6.4 Reduced Glutathione (GSH) Assay

Reduced glutathione (GSH) concentration was determined according to the method of Ellman (1959) using 5,5'-dithiobis-(2-nitrobenzoic acid) (DTNB).[25] The assay is based on the reaction of reduced glutathione with DTNB to produce the yellow-coloured 5-thio-2-nitrobenzoic acid (TNB), the intensity of which is directly proportional to the GSH concentration and is measured spectrophotometrically at 420 nm.

Briefly, 1.0 mL of the assay filtrate was mixed with 3.0 mL of phosphate buffer and 0.5 mL of Ellman's reagent (DTNB), followed by incubation at room temperature for 15 min. The absorbance of the resulting, yellow-coloured reaction product was measured at 420 nm using a UV–Visible spectrophotometer. A series of GSH standards (10–50 µg) was prepared and treated identically, while a reagent blank containing 1.0 mL of distilled water in place of the sample was included for background correction. Reduced glutathione concentration was determined from the calibration curve and expressed as mg g^{-1}.

2.7 Statistical Analysis

Biochemical assay responses were calculated from the recorded absorbance values using the assay-specific equations described above. Antioxidant activity was expressed as percentage inhibition for lipid peroxidation and as calculated activity or concentration values for SOD, CAT and GSH assays. The antioxidant data are presented descriptively across the tested concentrations to show concentration-dependent response patterns. Because the available experimental dataset did not include replicate-level measurements, no inferential statistical analyses were performed.

3. Results and Discussion

3.1 Formation of Silver Nanoparticles: Visual Observation and UV–Visible Spectroscopic Analysis

The formation of silver nanoparticles (AgNPs) was initially confirmed through visual observation of a distinct colour change following the addition of *Solanum aethiopicum* leaf extract to aqueous silver nitrate solution. The reaction mixture gradually changed from a greenish-yellow colour to dark brown, indicating the reduction of silver ions (Ag^+) to metallic silver nanoparticles (Ag^0). Such colour development is widely recognised as a preliminary indicator of AgNP formation and is attributed to surface plasmon resonance (SPR), arising from the collective oscillation of conduction-band electrons on the nanoparticle surface upon interaction with visible light. Plant-mediated AgNP synthesis commonly exhibits similar colour transitions, reflecting successful nanoparticle nucleation and growth.[11, 15]

As shown in Fig. 1, UV–Visible spectroscopic analysis provided further confirmation of nanoparticle formation. The synthesised AgNPs exhibited a strong absorption maximum centred at approximately 420 nm, corresponding to the characteristic surface plasmon resonance (SPR) band of silver nanoparticles. Similar absorption maxima within the range of 410–450 nm have been reported for plant-mediated AgNP systems and are commonly associated with the surface plasmon resonance of nanoscale silver particles.[11, 26] The relatively well-defined SPR band supports successful nanoparticle formation and provides limited optical evidence against extensive aggregation under the measurement conditions.

No prominent secondary absorption bands were observed within the 350–380 nm region of the spectrum. This indicates that the optical response was dominated by the principal AgNP surface plasmon resonance band. However, UV–Visible spectroscopy alone cannot establish particle monodispersity, exclude minor nanoparticle populations or confirm colloidal stability. Direct evaluation of dispersion stability would require complementary measurements such as hydrodynamic diameter, polydispersity index, zeta potential and time-dependent spectral monitoring.

The SPR position is influenced by particle size, morphology, dielectric environment, and degree of aggregation. Consequently, the observed absorption profile indicates efficient reduction of Ag^+ ions by phytochemicals present in *S. aethiopicum* leaves, including phenolic compounds, flavonoids, tannins,

alkaloids, and reducing sugars, which likely functioned as both reducing and stabilising agents during nanoparticle formation. [11, 15] The optical characteristics therefore provide evidence for successful biosynthesis of AgNPs with a comparatively well-defined surface plasmon resonance response. Direct confirmation of colloidal stability would require additional dispersion and surface-charge measurements.

3.2 FTIR Analysis of Phytochemical-Mediated Reduction and Stabilisation

Fourier-transform infrared (FTIR) spectroscopy was employed to identify the functional groups involved in the biosynthesis and stabilisation of silver nanoparticles and to provide insight into the phytochemical constituents responsible for nanoparticle formation. FTIR analysis is widely used in green nanotechnology to elucidate interactions between plant-derived biomolecules and metallic nanoparticles because phytochemicals often function simultaneously as reducing agents and stabilising ligands during nanoparticle synthesis.[11, 15]

Table 1
FTIR absorption bands of biosynthesised silver nanoparticles synthesised using *Solanum aethiopicum* leaf extract and their corresponding functional group assignments.

Wavenumber (cm^{-1})	Peak Intensity	Functional Group	Bond Type	Origin
3432	Broad, Strong	O-H stretch	Hydroxyl groups	Phenolics, alcohols from plant extract
2924	Medium	C-H stretch	Alkyl groups	Phytochemicals
2854	Medium	C-H stretch	Methylene groups	Lipids, fatty acids
1635	Strong	C = O stretch	Amide I band	Proteins/peptides (capping agents)
1516	Medium	C = C stretch	Aromatic ring	Flavonoids, phenolic compounds
1384	Medium	C-N stretch	Aromatic amines	Alkaloids from S. aethiopicum
1076	Strong	C-O stretch	Ether/ester linkage	Polysaccharides, glycosides
618	Weak	Ag-O	Metal-oxygen	Silver nanoparticle interaction

The FTIR spectrum of the biosynthesised AgNPs displayed prominent absorption bands at 3432, 2924, 2854, 1635, 1516, 1384, 1076, and 618 cm^{-1} (Fig. 2; Table 1). The broad and intense absorption band observed at 3432 cm^{-1} corresponds to O–H stretching vibrations of hydroxyl-containing compounds, including phenolic compounds and alcohols. Such compounds are abundant in plant extracts and are frequently implicated in the reduction of silver ions because of their electron-donating capacity. The

absorption bands at 2924 and 2854 cm^{-1} are attributable to aliphatic C–H stretching vibrations associated with alkyl and methylene groups, indicating the presence of lipidic and other hydrocarbon-containing phytoconstituents.

The strong band observed at 1635 cm^{-1} is assigned to C = O stretching vibrations of amide functionalities (amide I region), suggesting the presence of proteins or peptide-derived biomolecules adsorbed on the nanoparticle surface. The peak at 1516 cm^{-1} corresponds to aromatic C = C stretching vibrations commonly associated with flavonoids and polyphenolic compounds, whereas the absorption band at 1384 cm^{-1} is attributed to C–N stretching vibrations of aromatic amines, indicating the possible involvement of alkaloid constituents present in *S. aethiopicum*. Furthermore, the strong absorption at 1076 cm^{-1} corresponds to C–O stretching vibrations of ether and ester linkages associated with polysaccharides, glycosides, and related oxygen-containing phytochemicals. A weak absorption band observed at 618 cm^{-1} may be attributed to Ag–O interactions, providing additional evidence for coordination between silver atoms and oxygen-containing functional groups on the nanoparticle surface.

The FTIR spectrum of the biosynthesised AgNPs contained absorption bands attributable to hydroxyl-, carbonyl-, aromatic-, amine- and ether-containing functional groups. These findings are consistent with the presence of plant-derived biomolecules associated with the nanoparticle surface. Similar functional groups have been reported in plant-mediated AgNP systems and are commonly associated with phytochemicals involved in nanoparticle reduction and surface capping.[18, 27] Direct confirmation of spectral shifts or changes in band intensity associated with nanoparticle formation would require comparison with the FTIR spectrum of the untreated *S. aethiopicum* leaf extract.

Collectively, the FTIR data support a phytochemical-mediated mechanism of nanoparticle synthesis in which hydroxyl-rich phenolic compounds and flavonoids may participate in the reduction of Ag^{+} ions to metallic Ag^{0} nanoparticles. Simultaneously, proteins, polysaccharides, alkaloids and other oxygen-containing biomolecules may adsorb onto the nanoparticle surface through interactions involving hydroxyl, carbonyl, amine and ether functionalities, thereby providing a plausible phytochemical capping layer that may limit particle–particle contact and aggregation. Similar reduction–capping mechanisms have been proposed for numerous biosynthesised silver nanoparticle systems.[11, 15, 28]

The retention of these phytochemicals on the nanoparticle surface is particularly significant from a biomedical perspective because the resulting phytochemical corona may substantially influence nanoparticle dispersion, surface reactivity, antioxidant performance, cellular uptake, and biological interactions. Increasing evidence suggests that the biological properties of green-synthesised AgNPs arise not solely from the metallic silver core but also from the synergistic contribution of surface-bound bioactive metabolites that modulate redox processes and cellular responses.[11, 12] Consequently, the FTIR findings provide important mechanistic support for the antioxidant activity observed in subsequent biochemical assays and reinforce the role of *S. aethiopicum* phytochemicals in generating biologically functionalised silver nanoparticles.

3.3 Transmission Electron Microscopy Analysis

Transmission electron microscopy (TEM) was employed to investigate the morphology, particle size, and dispersion characteristics of the biosynthesised silver nanoparticles.

TEM analysis revealed that the biosynthesised AgNPs were predominantly spherical, with most particles appearing individually dispersed, although mild local agglomeration was evident in some regions of the micrograph (Fig. 3). Such agglomeration is commonly observed in metallic nanoparticles and may arise from interparticle attractive forces or drying during TEM sample preparation. The predominantly spherical morphology is characteristic of many plant-mediated silver nanoparticles and is generally attributed to isotropic growth during phytochemical-assisted nanoparticle nucleation and crystal growth. Similar morphologies have been widely reported for green-synthesised AgNPs prepared using medicinal plant extracts.[29–31]

The two annotated nanoparticles exhibited approximate diameters of 9.22 and 12.54 nm (Fig. 3), consistent with the 10 nm scale bar and confirming the formation of nanoscale AgNPs. These dimensions are comparable to those reported for other biosynthesised silver nanoparticles.[30, 32] However, because only two particles were measured in the available TEM micrograph, these values should be regarded as representative particle dimensions rather than a statistically derived particle-size distribution. Although the TEM image suggests some variation in particle dimensions across the observed field, a quantitative assessment of particle-size distribution was not performed because measurements from a sufficiently large particle population and statistical analysis were unavailable.

Nevertheless, the observed particle dimensions are consistent with the nanoscale morphology evident in the TEM image and with the average crystallite size estimated by X-ray diffraction. Smaller nanoparticles generally possess a higher surface-area-to-volume ratio, which may enhance surface reactivity, catalytic performance and interactions with biological targets.[30, 32]

This morphology is consistent with the presence of surface-associated phytochemicals identified by FTIR, but TEM imaging alone cannot establish colloidal stability in suspension. Such stabilisation is consistent with the FTIR results, which demonstrated the presence of hydroxyl-, carbonyl-, amine-, and ether-containing biomolecules capable of acting as capping agents.

From a biomedical perspective, the relatively small particle size observed in the present study is noteworthy because nanoparticles within the 10–20 nm range often exhibit enhanced biological performance due to increased surface accessibility and improved interaction with biomolecules, cellular membranes, and reactive oxygen species.[9, 33] Smaller nanoparticles generally possess a higher surface-area-to-volume ratio, which may increase surface reactivity. The biological significance of the observed particle dimensions and mild agglomeration would require confirmation using appropriate cellular and dispersion-stability studies. The balance between nanoscale activity and physicochemical stability is particularly important in nanomedicine applications because it can influence antioxidant efficacy, biodistribution, cellular uptake, and eventual therapeutic selectivity.

Overall, the TEM findings confirm the formation of predominantly spherical nanoscale silver particles with mild local agglomeration. When considered together with the UV–Vis, FTIR and XRD data, the results support the production of crystalline, phytochemically capped AgNPs with physicochemical characteristics that justify further investigation in antioxidant and oxidative stress-related biomedical models.

3.4 Crystalline Structure and Phase Composition by XRD

The crystalline nature and phase composition of the biosynthesised silver nanoparticles (AgNPs) were investigated using X-ray diffraction (XRD) analysis.

Table 2
Crystallographic parameters and crystallite size of biosynthesised silver nanoparticles calculated from XRD diffraction peaks using the Debye–Scherrer equation.

Peak (hkl)	2θ (°)	FWHM (°)	FWHM (rad)	Crystallite Size (nm)
(111)	38.12	0.48	0.00838	17.5
(200)	44.28	0.52	0.00908	16.4
(220)	64.43	0.58	0.01012	15.8
(311)	77.39	0.61	0.01065	16.2

The XRD pattern exhibited four prominent diffraction peaks at 2θ values of 38.12°, 44.28°, 64.43° and 77.39°, corresponding to the (111), (200), (220) and (311) crystallographic planes of face-centred cubic (fcc) silver (Fig. 4). These reflections were indexed to the standard diffraction pattern for metallic silver (JCPDS Card No. 04-0783), confirming the successful biosynthesis of crystalline metallic AgNPs[18]. Similar diffraction patterns have been widely reported for plant-mediated silver nanoparticles and are considered characteristic of the reduction of Ag^+ ions to crystalline Ag^0 nanostructures.[11] No additional prominent diffraction peaks attributable to crystalline impurity phases or silver oxide were observed, indicating that no major crystalline impurity phases were detected under the experimental conditions. Although phytochemical capping agents remain associated with the nanoparticle surface, these organic constituents are predominantly amorphous and therefore contribute minimally to the diffraction pattern.

The average crystallite size, calculated using the Debye–Scherrer equation, was 16.5 ± 0.7 nm. Individual crystallite sizes calculated from the principal reflections ranged from 15.8 to 17.5 nm (Table 2), demonstrating good agreement across the major diffraction peaks and confirming the nanoscale crystalline nature of the biosynthesised AgNPs. The dominant intensity of the (111) reflection further supports the preferential crystallographic orientation typically observed for face-centred cubic silver nanoparticles synthesised by green methods.

The crystallite size determined by XRD was slightly larger than the particle dimensions observed by TEM (approximately 9.22–12.54 nm). This difference is expected because XRD estimates the size of coherent

crystalline domains, whereas TEM measures the physical dimensions of individual nanoparticles. Although the TEM particle dimensions and XRD crystallite size differ, both confirm that the synthesised material is within the nanoscale range. The difference is expected because XRD estimates coherent crystalline domains whereas TEM measures the physical dimensions of individual particles.

Crystallinity is an important physicochemical characteristic because it influences nanoparticle stability, optical behaviour, catalytic activity, surface reactivity and biological interactions. Highly crystalline AgNPs possess well-defined crystal facets that facilitate electron-transfer processes and redox reactions, properties that may contribute to the pronounced antioxidant activity observed in the present study.[12] Collectively, the XRD findings demonstrate that *S. aethiopicum*-mediated biosynthesis produced highly crystalline AgNPs with no major crystalline impurity phases detected by XRD. These structural characteristics support their suitability for further investigation in oxidative stress-related biomedical applications.

3.5 Structure–Activity Relationship of Biosynthesised AgNPs

A major objective in nanomedicine research is to establish clear relationships between the physicochemical characteristics of nanoparticles and their biological performance. The collective characterisation results obtained in the present study suggest that the antioxidant activity of the biosynthesised *Solanum aethiopicum*-derived AgNPs is influenced by the combined effects of particle size, morphology, crystallinity, optical properties, and phytochemical surface functionalisation. Rather than acting independently, these physicochemical characteristics are likely to function synergistically in determining the biological behaviour of the nanoparticles.[9, 33]

UV–Visible spectroscopy confirmed nanoparticle formation through the characteristic surface plasmon resonance band centred at approximately 420 nm. No prominent secondary absorption bands were observed within the 350–380 nm region, indicating that the optical response was dominated by the principal AgNP surface plasmon resonance band. These optical characteristics are consistent with successful nanoparticle formation and a comparatively well-defined optical response, as commonly reported for plant-mediated AgNP systems.[11, 15] However, direct assessment of particle-size distribution and colloidal stability would require complementary measurements such as dynamic light scattering, hydrodynamic diameter, polydispersity index, zeta potential and time-dependent stability analysis.

TEM analysis showed two representative particle diameters of approximately 9.22 and 12.54 nm, while XRD analysis yielded an average crystallite size of approximately 16.5 nm. Nanoparticles within this size range possess a high surface-area-to-volume ratio, increasing the proportion of surface atoms available for interactions with surrounding molecules. Such nanoscale dimensions have frequently been associated with improved biological activity, including antioxidant performance, owing to enhanced accessibility of reactive surface sites. [9, 12, 33]

The crystalline nature of the nanoparticles was confirmed by diffraction peaks corresponding to the (111), (200), (220), and (311) crystallographic planes of face-centred cubic silver, which matched the standard diffraction pattern reported in JCPDS Card No. 04-0783. The absence of additional diffraction peaks indicates that the synthesised nanoparticles were predominantly composed of crystalline metallic silver with minimal detectable crystalline impurities. Similar diffraction patterns have been widely reported for biosynthesised AgNPs prepared using plant extracts.[11, 34]

FTIR analysis demonstrated that hydroxyl, carbonyl, aromatic, amine, and ether-containing functional groups remained associated with the nanoparticle surface following synthesis. These functional groups are characteristic of phenolics, flavonoids, proteins, alkaloids, polysaccharides, and related phytochemicals naturally present in *S. aethiopicum* leaf extract. Their persistence after nanoparticle formation supports their dual role as reducing agents during Ag^+ reduction and as capping agents responsible for nanoparticle stabilisation. Phytochemical capping has been reported to improve nanoparticle dispersion, reduce aggregation, and contribute to the biological activity of green-synthesised AgNPs through the retention of bioactive surface functionalities.[11, 15, 28]

The physicochemical characteristics observed in the present study provide a plausible explanation for the antioxidant-associated responses demonstrated by the biosynthesised AgNPs. The pronounced inhibition of lipid peroxidation together with the concentration-associated changes in the calculated SOD, CAT and GSH assay responses suggests that the nanoparticles may exert antioxidant-associated effects under the assay conditions through complementary mechanisms involving interactions with reactive oxygen species and endogenous antioxidant defence systems. Because the biochemical data were derived from single calculated values without replicate-level measurements, these mechanistic interpretations remain provisional. Similar structure–activity relationships have been reported for other plant-mediated AgNPs, in which the combined influence of nanoscale dimensions and phytochemical surface coatings contributes to enhanced antioxidant performance.[11, 12]

Overall, the present findings suggest a possible structure–activity relationship in which nanoscale particle dimensions, crystalline metallic silver, predominantly spherical morphology and phytochemical surface capping may collectively contribute to the observed antioxidant-associated responses. Although colloidal stability, surface charge and hydrodynamic particle size were not directly assessed, the combined physicochemical and biochemical findings support further investigation of these phytochemically capped AgNPs in oxidative stress-related biomedical models, including appropriately designed cellular and animal studies of oxidative stress and cancer.[7, 8]

3.6 In Vitro Antioxidant Activity

3.6.1 Inhibition of Lipid Peroxidation (MDA)

Lipid peroxidation is a major consequence of oxidative stress and occurs when reactive oxygen species attack polyunsaturated fatty acids in biological membranes. This process generates malondialdehyde (MDA), a reactive aldehydic product widely used as an index of oxidative membrane damage. In the

thiobarbituric acid reactive substances assay, MDA reacts with thiobarbituric acid to form a coloured MDA–TBA adduct, and reduced formation of this adduct reflects inhibition of lipid peroxidation. The ability of the biosynthesised AgNPs to suppress MDA formation was therefore used as an indicator of lipid peroxidation inhibitory activity.

Table 3
Inhibition of malondialdehyde (MDA) formation by biosynthesised *Solanum aethiopicum* AgNPs and ascorbic acid at different concentrations.

Sample	Concentration (mg mL^{-1})	MDA Inhibition (%)
AgNPs	2	94.48
AgNPs	4	95.23
AgNPs	6	96.07
Ascorbic acid	2	82.26
Ascorbic acid	4	90.79
Ascorbic acid	6	90.54

Values are calculated percentage inhibition values derived from the recorded absorbance data. Ascorbic acid was used as the reference antioxidant.

As shown in Table 3, the biosynthesised AgNPs produced high inhibition of lipid peroxidation across the tested concentrations, with MDA inhibition values of 94.48%, 95.23% and 96.07% at 2, 4 and 6 mg mL^{-1}, respectively. Under the same assay conditions, ascorbic acid produced inhibition values of 82.26%, 90.79% and 90.54% at the corresponding concentrations. These results indicate that the AgNP preparation strongly suppressed MDA formation in the liver-homogenate lipid peroxidation model.

The inhibition of MDA formation suggests that the biosynthesised AgNPs reduced oxidative degradation of membrane lipids under the assay conditions. This activity may be associated with the combined contribution of the silver nanoparticle core and the phytochemical capping layer derived from *S. aethiopicum* leaf extract. Plant-mediated AgNPs have been reported to exhibit antioxidant activity through mechanisms involving nanoscale surface reactivity, electron-transfer processes and the contribution of surface-bound phytochemicals.[11, 12] The FTIR analysis supports the presence of hydroxyl, carbonyl, aromatic, amine and ether-containing phytochemical groups on the nanoparticle surface, which may contribute to redox activity, stabilisation of radical intermediates and interruption of lipid peroxidation chain reactions.[11, 12] However, because the antioxidant data are presented as calculated assay responses derived from recorded absorbance values, the observed differences should be interpreted descriptively rather than as statistically confirmed differences between AgNPs and ascorbic acid.

3.6.2 Superoxide Dismutase (SOD) Activity

Superoxide dismutase (SOD) constitutes a primary enzymatic defence against oxidative stress by catalysing the conversion of superoxide radicals into hydrogen peroxide and molecular oxygen.

Table 4
Superoxide dismutase (SOD) activity following treatment with biosynthesised *Solanum aethiopicum* silver nanoparticles.

Concentration (mg mL^{-1})	Calculated SOD activity (10^{-6} U mL^{-1})
2	2.49
6	7.46
8	6.22

Values are presented as calculated assay responses derived from the recorded absorbance data.

As shown in Table 4, the calculated SOD activities were 2.49, 7.46 and 6.22 × 10^{-6} U mL^{-1} at AgNP concentrations of 2, 6 and 8 mg mL^{-1}, respectively. The highest calculated SOD activity was observed at 6 mg mL^{-1}, followed by a lower value at 8 mg mL^{-1}.

SOD constitutes a primary antioxidant defence enzyme that catalyses the dismutation of superoxide radicals into hydrogen peroxide and molecular oxygen.[35, 36] The SOD activity pattern observed in this study suggests that the biosynthesised AgNPs may influence superoxide-associated antioxidant responses under the assay conditions. The lower value observed at 8 mg mL^{-1} compared with 6 mg mL^{-1} suggests an apparent optimum at the intermediate concentration. This response may reflect concentration-dependent interactions between the phytochemical-capped AgNP surface and reactive oxygen species or antioxidant enzyme systems. However, because the available SOD data are calculated assay responses derived from absorbance changes rather than replicate-level datasets, these trends should be interpreted descriptively rather than as statistically confirmed enzyme-modulatory effects.

3.6.3 Catalase Activity

Catalase (CAT) functions synergistically with SOD by catalysing the decomposition of hydrogen peroxide into water and oxygen, thereby preventing the formation of highly reactive hydroxyl radicals.

Table 5
Catalase (CAT) activity following treatment with biosynthesised *Solanum aethiopicum* silver nanoparticles.

Concentration (mg mL^{-1})	Calculated catalase activity (U mL^{-1})
2	26.84
6	28.82
8	25.52

Values are presented as calculated catalase activities derived from recorded absorbance data. CAT, catalase.

As shown in Table 5, catalase activity was recorded as 26.84, 28.82 and 25.52 U mL^{-1} at 2, 6 and 8 mg mL^{-1}, respectively. The highest calculated catalase activity was observed at 6 mg mL^{-1}, followed by a lower value at 8 mg mL^{-1}.

Catalase plays a complementary role to SOD in antioxidant defence by decomposing hydrogen peroxide into water and oxygen, thereby limiting the formation of highly reactive hydroxyl radicals. [37] The catalase response observed in this study, together with the SOD activity pattern, suggests that the biosynthesised AgNPs may influence enzyme-associated antioxidant pathways under the assay conditions. The maximal CAT and SOD responses at 6 mg mL^{-1} further suggest a concentration-dependent response pattern with an apparent optimum at the intermediate concentration. This behaviour may reflect interactions between the phytochemical-capped AgNP surface and reactive oxygen species or antioxidant enzyme systems. However, because the available antioxidant data are calculated assay responses rather than replicate-level datasets, these trends should be interpreted descriptively rather than as statistically confirmed enzyme-modulatory effects.

3.6.4 Reduced Glutathione (GSH) Levels

Reduced glutathione (GSH) is one of the most important non-enzymatic antioxidants in biological systems and plays a central role in maintaining intracellular redox balance.

Table 6
Reduced glutathione (GSH) concentration following treatment with biosynthesised *Solanum aethiopicum* silver nanoparticles.

Concentration (mg mL^{-1})	GSH (mg g^{-1})
2	0.162
6	0.342
8	0.453

Values are presented as calculated GSH concentrations derived from recorded absorbance data. GSH, reduced glutathione.

As shown in Table 6, calculated GSH values increased from 0.162 mg g^{-1} at 2 mg mL^{-1} to 0.342 mg g^{-1} at 6 mg mL^{-1} and 0.453 mg g^{-1} at 8 mg mL^{-1}. This pattern indicates a concentration-dependent increase in the calculated GSH response across the tested AgNP concentrations.

GSH is a major non-enzymatic antioxidant involved in reactive oxygen species detoxification, maintenance of thiol–disulfide balance and protection against oxidative damage to biomolecules[5, 6, 38] The observed increase in calculated GSH values suggests that the biosynthesised AgNPs may support

reduced-glutathione-associated antioxidant capacity under the assay conditions. This response complements the calculated SOD and CAT activity patterns and supports the broader antioxidant profile of the phytochemical-capped AgNPs. However, because the available GSH data are calculated assay responses rather than replicate-level datasets, this trend should be interpreted descriptively rather than as statistically confirmed enhancement of GSH status.

3.7 Proposed Antioxidant Mechanism and Biomedical Relevance

The collective physicochemical and biochemical findings support the mechanistic model illustrated in Fig. 5, in which phytochemical-capped AgNPs synthesised from *S. aethiopicum* function as redox-active nanostructures. During nanoparticle formation, phenolics, flavonoids, tannins, alkaloids and related phytochemicals reduce Ag^+ ions to Ag^0 while simultaneously adsorbing onto the nanoparticle surface as stabilising agents. The resulting phytochemical corona may influence nanoparticle surface interactions and antioxidant-associated behaviour; however, its contribution to colloidal stability was not directly assessed.

The strong inhibition of lipid peroxidation, together with the measured SOD, CAT and GSH responses, suggests that the biosynthesised nanoparticles exert antioxidant effects through multiple complementary pathways. These include direct scavenging of reactive oxygen species, interruption of free-radical chain reactions, stabilisation of reactive intermediates, and reinforcement of endogenous antioxidant defences. The observed activity is likely attributable to the synergistic interaction between the metallic nanoparticle core and the bioactive phytochemical coating.

The ability of *S. aethiopicum*-derived AgNPs to modulate multiple antioxidant pathways suggests potential utility as redox-active nanomaterials for future biomedical applications. Previous studies have shown that phytochemical-mediated AgNPs can induce ROS-mediated apoptosis and cytotoxicity in cancer cells; however, these effects were not evaluated in the present study and therefore require confirmation using appropriate cancer-cell models.[18, 39] Furthermore, comprehensive toxicological evaluation remains essential because silver nanoparticles may exhibit dose-dependent cytotoxicity in mammalian systems, despite evidence that green-synthesised AgNPs may show improved biocompatibility than chemically synthesised nanoparticles.[19]

4. Conclusion

This study demonstrates that aqueous leaf extract of *Solanum aethiopicum* can serve as an effective and sustainable reducing and stabilising agent for the green synthesis of silver nanoparticles with well-defined physicochemical characteristics and pronounced antioxidant-associated responses under the assay conditions. Successful nanoparticle formation was confirmed by visual observation, UV–Visible spectroscopy, FTIR spectroscopy, TEM and X-ray diffraction analyses, which collectively demonstrated the formation of predominantly spherical, crystalline AgNPs with nanoscale dimensions and

phytochemical surface functionalisation. The combined characterisation findings indicate that plant-derived biomolecules played essential roles in both the reduction of Ag^+ ions and stabilisation of the resulting nanoparticles.

The biosynthesised AgNPs exhibited pronounced antioxidant activity, as evidenced by strong inhibition of lipid peroxidation together with enhanced superoxide dismutase, catalase, and reduced glutathione activities. The collective physicochemical and biochemical findings suggest that the antioxidant performance of the nanoparticles is closely associated with their nanoscale dimensions, crystalline structure, colloidal characteristics, and phytochemical surface corona, highlighting the importance of structure–activity relationships in plant-mediated nanomaterials.

Although the present study did not include cancer cell-based experiments, the observed antioxidant properties suggest potential relevance for future nanomedicine applications involving oxidative stress-associated diseases. Further investigations should include comprehensive physicochemical characterisation, in vitro cytotoxicity studies using normal and cancer cell lines, mechanistic analyses of intracellular redox pathways, and *in vivo* safety and efficacy evaluations. Collectively, these findings provide a strong foundation for future evaluation of *S. aethiopicum*-derived silver nanoparticles in relevant cellular and in vivo disease models.

5. Study limitations and future perspectives

The present study has several limitations. The biological evaluation was limited to *in vitro* antioxidant assays using a rat liver homogenate model and therefore does not fully reflect cellular or *in vivo* biological responses. In addition, no cancer cell-based experiments were performed; consequently, any implications regarding the anticancer potential of *Solanum aethiopicum*-derived AgNPs remain prospective. The study also did not include a comparison with chemically synthesised AgNPs or additional colloidal characterisation, such as hydrodynamic particle size, zeta potential, polydispersity index, and long-term stability, which are important determinants of nanoparticle behaviour in biological systems.[11, 15] Furthermore, toxicity and biocompatibility were not evaluated in normal mammalian cells or *in vivo* models, limiting assessment of the translational potential of the biosynthesised nanoparticles.[19] In addition, the antioxidant responses were calculated from the available experimental dataset, which did not include replicate measurements. Consequently, inferential statistical comparisons between treatments were not performed, and the observed differences should therefore be interpreted as descriptive trends rather than statistically confirmed effects.

Future studies should validate these findings in representative cancer and normal cell lines, investigate the underlying molecular mechanisms of antioxidant and potential anticancer activity, and expand nanoparticle characterisation using techniques such as dynamic light scattering, zeta potential analysis, and energy-dispersive X-ray spectroscopy.[11, 15] Well-designed *in vivo* studies evaluating biodistribution, pharmacokinetics, pharmacodynamics, long-term toxicity, and therapeutic efficacy will also be necessary before clinical translation can be considered.[19]

Declarations

Conflict of Interest:

The authors declare that they have no competing interests.

Ethics Approval:

All animal procedures were conducted in accordance with institutional guidelines and were approved by the Research Ethics Committee of the Department of Biochemistry, Faculty of Basic Medical Sciences, Federal University of Allied Health Sciences, Enugu State.

Funding:

This research received no specific grant from any funding agency in the public, commercial or not-for-profit sectors.

Author Contribution

C.P.O. conceived and supervised the study and provided the necessary resources. M.C.O. and A.A.A. carried out the experimental work and participated in data collection. J.O.N. performed the biochemical analyses and contributed to data curation. B.C.A. assisted with validation of the findings and reviewed the manuscript. J.I.A. conducted the formal analysis, reviewed and validated the data, prepared the original manuscript draft, revised and edited subsequent versions, and served as a corresponding author alongside C.P.O. All authors read and approved the final manuscript.

Data Availability

The data supporting the findings of this study are included within the article. Additional data are available from the corresponding authors upon reasonable request.

References

1. Ayogu JI, Odoh AS (2020) Prospects and therapeutic applications of cardiac glycosides in cancer remediation. ACS Comb Sci 22(11):543–553
2. Sung H, Ferlay J, Siegel RL, Laversanne M, Soerjomataram I, Jemal A, Bray F (2021) Global cancer statistics 2020: GLOBOCAN estimates of incidence and mortality worldwide for 36 cancers in 185 countries. CA Cancer J Clin 71(3):209–249

3. Bray F, Laversanne M, Sung H, Ferlay J, Siegel RL, Soerjomataram I, Jemal A (2024) Global cancer statistics 2022: GLOBOCAN estimates of incidence and mortality worldwide for 36 cancers in 185 countries. CA Cancer J Clin 74(3):229–263
4. Siegel RL, Giaquinto AN, Jemal A (2024) Cancer statistics, 2024. CA Cancer J Clin 74(1):12–49
5. Liguori I, Russo G, Curcio F, Bulli G, Aran L, Della-Morte D, Gargiulo G, Testa G, Cacciatore F, Bonaduce D (2018) Oxidative stress, aging, and diseases. Clin Interv Aging 757–772
6. Sies H, Jones DP (2020) Reactive oxygen species (ROS) as pleiotropic physiological signalling agents. Nat Rev Mol Cell Biol 21(7):363–383
7. Hayes JD, Dinkova-Kostova AT, Tew K (2020) D. Oxidative stress in cancer. Cancer Cell 38(2):167–197
8. Reczek CR, Chandel NS (2017) The two faces of reactive oxygen species in cancer. Annu Rev Cancer Biol 1:79–98
9. Bayda S, Adeel M, Tuccinardi T, Cordani M, Rizzolio F (2019) The history of nanoscience and nanotechnology: from chemical–physical applications to nanomedicine. Molecules 25(1):112
10. Ventola CL (2017) Progress in nanomedicine: approved and investigational nanodrugs. Pharm Ther 42(12):742
11. Adeyemi JO, Oriola AO, Onwudiwe DC, Oyedeji AO (2022) Plant extracts mediated metal-based nanoparticles: synthesis and biological applications. Biomolecules 12(5):627
12. Bedlovičová Z, Strapáč I, Baláž M, Salayová A (2020) A brief overview on antioxidant activity determination of silver nanoparticles. Molecules 25(14):3191
13. Magdy G, Aboelkassim E, Abd Elhaleem SM, Belal F (2024) A comprehensive review on silver nanoparticles: Synthesis approaches, characterization techniques, and recent pharmaceutical, environmental, and antimicrobial applications. Microchem J 196:109615
14. Abid N, Khan AM, Shujait S, Chaudhary K, Ikram M, Imran M, Haider J, Khan M, Khan Q, Maqbool M (2022) Synthesis of nanomaterials using various top-down and bottom-up approaches, influencing factors, advantages, and disadvantages: A review. Adv Colloid Interface Sci 300:102597
15. Jadoun S, Arif R, Jangid NK, Meena RK (2021) Green synthesis of nanoparticles using plant extracts: A review. Environ Chem Lett 19(1):355–374
16. Shaikh WA, Chakraborty S, Owens G, Islam RU (2021) A review of the phytochemical mediated synthesis of AgNP (silver nanoparticle): the wonder particle of the past decade. Appl Nanosci 11(11):2625–2660
17. Taher D, Solberg SØ, Prohens J, Chou Y-y, Rakha M, Wu T (2017) -h. World vegetable center eggplant collection: origin, composition, seed dissemination and utilization in breeding. Front Plant Sci 8:279838
18. Kumari SA, Patlolla AK, Madhusudhanachary P (2022) Biosynthesis of silver nanoparticles using Azadirachta indica and their antioxidant and anticancer effects in cell lines. Micromachines 13(9):1416

19. Jaswal T, Gupta J (2023) A review on the toxicity of silver nanoparticles on human health. *Mater. Today Proc. 81*, 859–863
20. Langford JI, Wilson A (1978) Scherrer after sixty years: a survey and some new results in the determination of crystallite size. J Appl Crystallogr 11(2):102–113
21. Ohkawa H, Ohishi N, Yagi K (1979) Assay for lipid peroxides in animal tissues by thiobarbituric acid reaction. Anal Biochem 95(2):351–358
22. Buege JA, Aust SD (1978) [30] Microsomal lipid peroxidation. In *Methods Enzymol.*, Vol. 52; Elsevier, ; pp 302–310
23. Sun M, Zigman S (1978) An improved spectrophotometric assay for superoxide dismutase based on epinephrine autoxidation. Anal Biochem 90(1):81–89
24. Sinha AK (1972) Colorimetric assay of catalase. Anal Biochem 47(2):389–394
25. Gl E (1959) Tissue sulfhydryl groups. Arch Biochem Biophys 82:70–77
26. Gamboa SM, Rojas ER, Martínez VV, Vega-Baudrit J (2019) Synthesis and characterization of silver nanoparticles and their application as an antibacterial agent. Int J Biosen Bioelectron 5(5):166–173
27. Patil RB, Chougale AD (2021) Analytical methods for the identification and characterization of silver nanoparticles: A brief review. *Mater. Today Proc. 47*, 5520–5532
28. Vishwanath R, Negi B (2021) Conventional and green methods of synthesis of silver nanoparticles and their antimicrobial properties. Curr Res Green Sustainable Chem 4:100205
29. Shankar SS, Rai A, Ahmad A, Sastry M (2004) Rapid synthesis of Au, Ag, and bimetallic Au core–Ag shell nanoparticles using Neem (Azadirachta indica) leaf broth. J Colloid Interface Sci 275(2):496–502
30. Okka EZ, Tongur T, Aytas TT, Yılmaz M, Topel Ö, Sahin R (2023) Green Synthesis and the formation kinetics of silver nanoparticles in aqueous Inula Viscosa extract. Optik 294:171487
31. Song JY, Kim BS (2009) Rapid biological synthesis of silver nanoparticles using plant leaf extracts. Bioprocess Biosyst Eng 32(1):79–84
32. Yang S (2021) Characterization of silver nanoparticles. Polymer Nanocomposites Based on Silver Nanoparticles: Synthesis, Characterization and Applications. Springer, pp 83–107
33. Gherasim O, Puiu RA, Bîrcă AC, Burdușel A-C, Grumezescu AM (2020) An updated review on silver nanoparticles in biomedicine. Nanomaterials 10(11):2318
34. Shnoudeh AJ, Hamad I, Abdo RW, Qadumii L, Jaber AY, Surchi HS, Alkelany SZ (2019) Synthesis, characterization, and applications of metal nanoparticles. Biomaterials and Bionanotechnology. Elsevier, pp 527–612
35. Liu W, Worms I, Slaveykova VI (2020) Interaction of silver nanoparticles with antioxidant enzymes. Environ Science: Nano 7(5):1507–1517
36. Matsuoka K, Nakatani Y, Yoshimura T, Akasaki T (2019) Superoxide scavenging activity of gold, silver, and platinum nanoparticles capped with sugar-based nonionic surfactants. J Oleo Sci 68(9):847–854

37. Ransy C, Vaz C, Lombès A, Bouillaud F (2020) Use of H2O2 to cause oxidative stress, the catalase issue. Int J Mol Sci 21(23):9149
38. Zorraquín-Peña I, Cueva C, de González D, Bartolomé B, Moreno-Arribas MV (2020) Glutathione-stabilised silver nanoparticles: antibacterial activity against periodontal bacteria, and cytotoxicity and inflammatory response in oral cells. Biomedicines 8(10):375
39. Ju S, Singh MK, Han S, Ranbhise J, Ha J, Choe W, Yoon K-S, Yeo SG, Kim SS, Kang I (2024) Oxidative stress and cancer therapy: controlling cancer cells using reactive oxygen species. Int J Mol Sci 25(22):12387

Figures

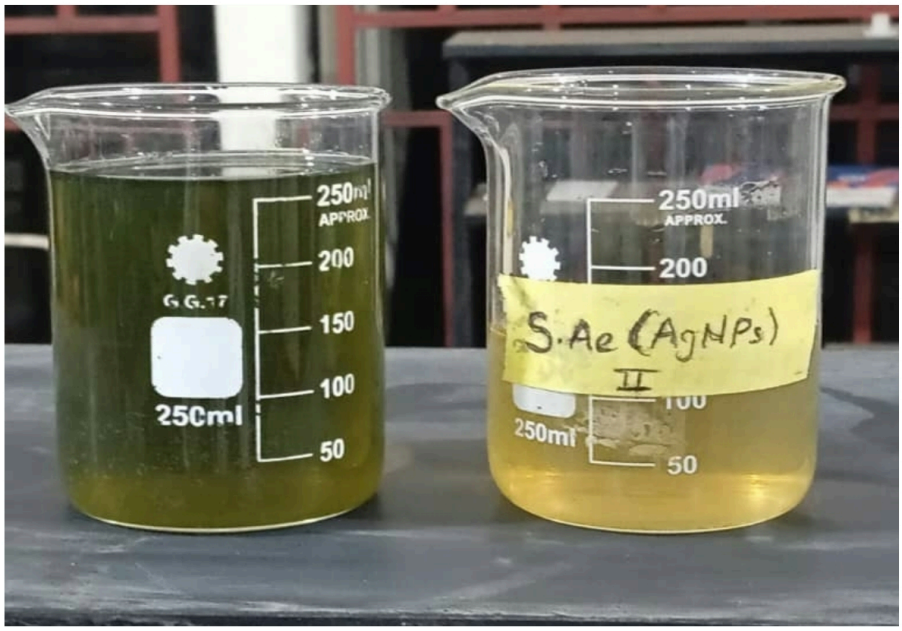

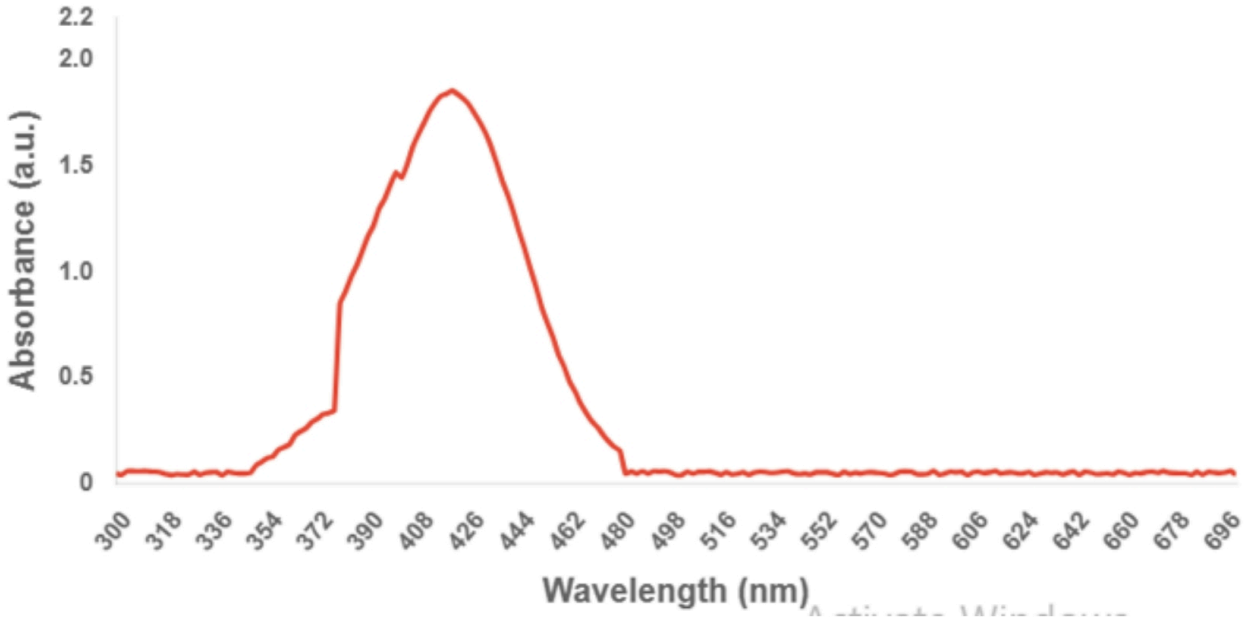

Figure 1

Visual observation of silver nanoparticle formation and UV–visible absorption spectrum of biosynthesised AgNPs from Solanum aethiopicum leaf extract. (A) Colour change accompanying reduction of Ag^+ ions during nanoparticle formation. (B) UV–visible spectrum showing the characteristic surface plasmon resonance band at approximately 420 nm.

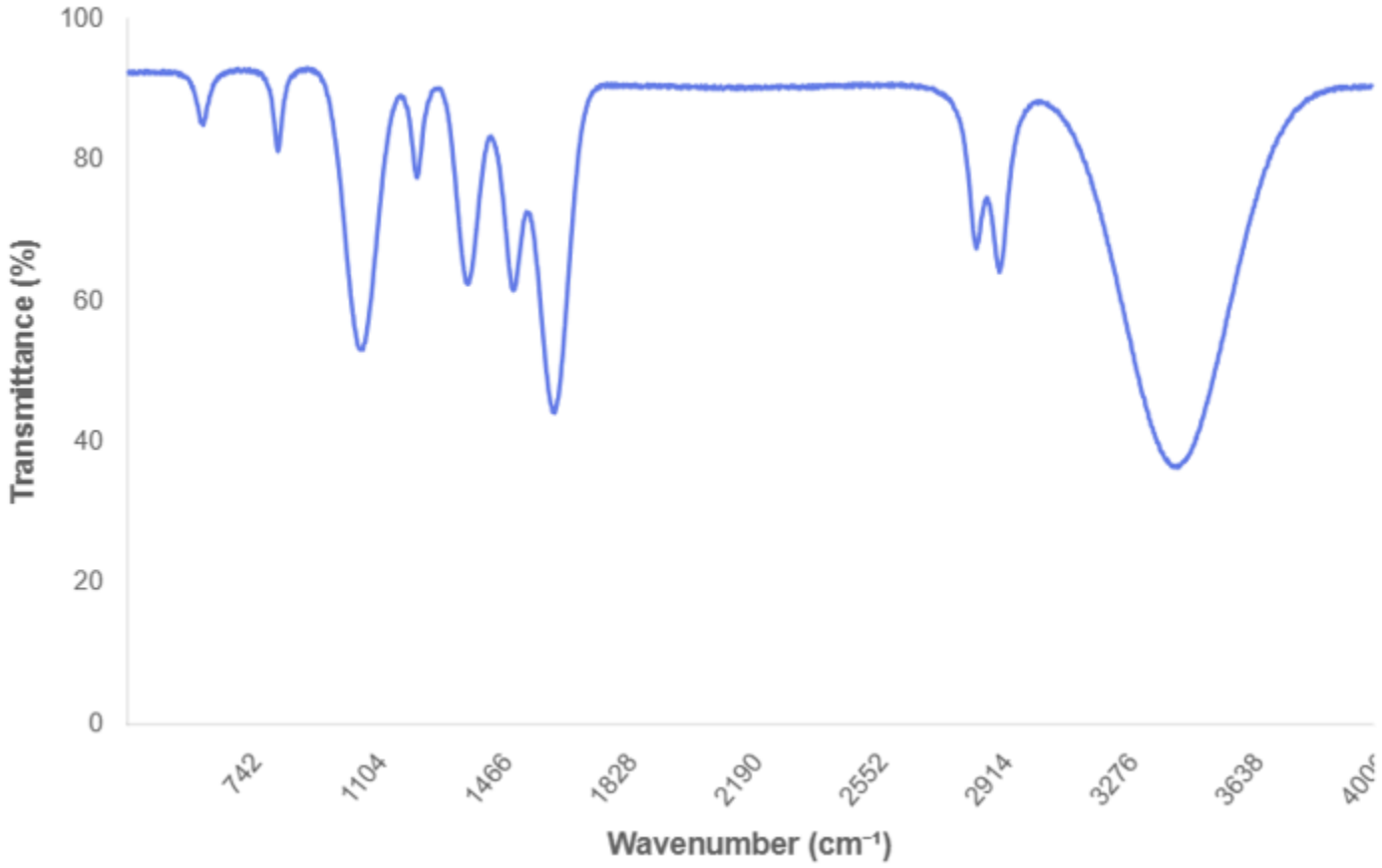

Figure 2

FTIR spectrum of biosynthesised AgNPs prepared using Solanum aethiopicum leaf extract. Major absorption bands at 3432, 2924, 2854, 1635, 1516, 1384, 1076 and 618 cm^{-1} indicate the participation of hydroxyl, aliphatic, carbonyl, aromatic, amine and ether-containing phytochemicals in nanoparticle reduction and stabilisation.

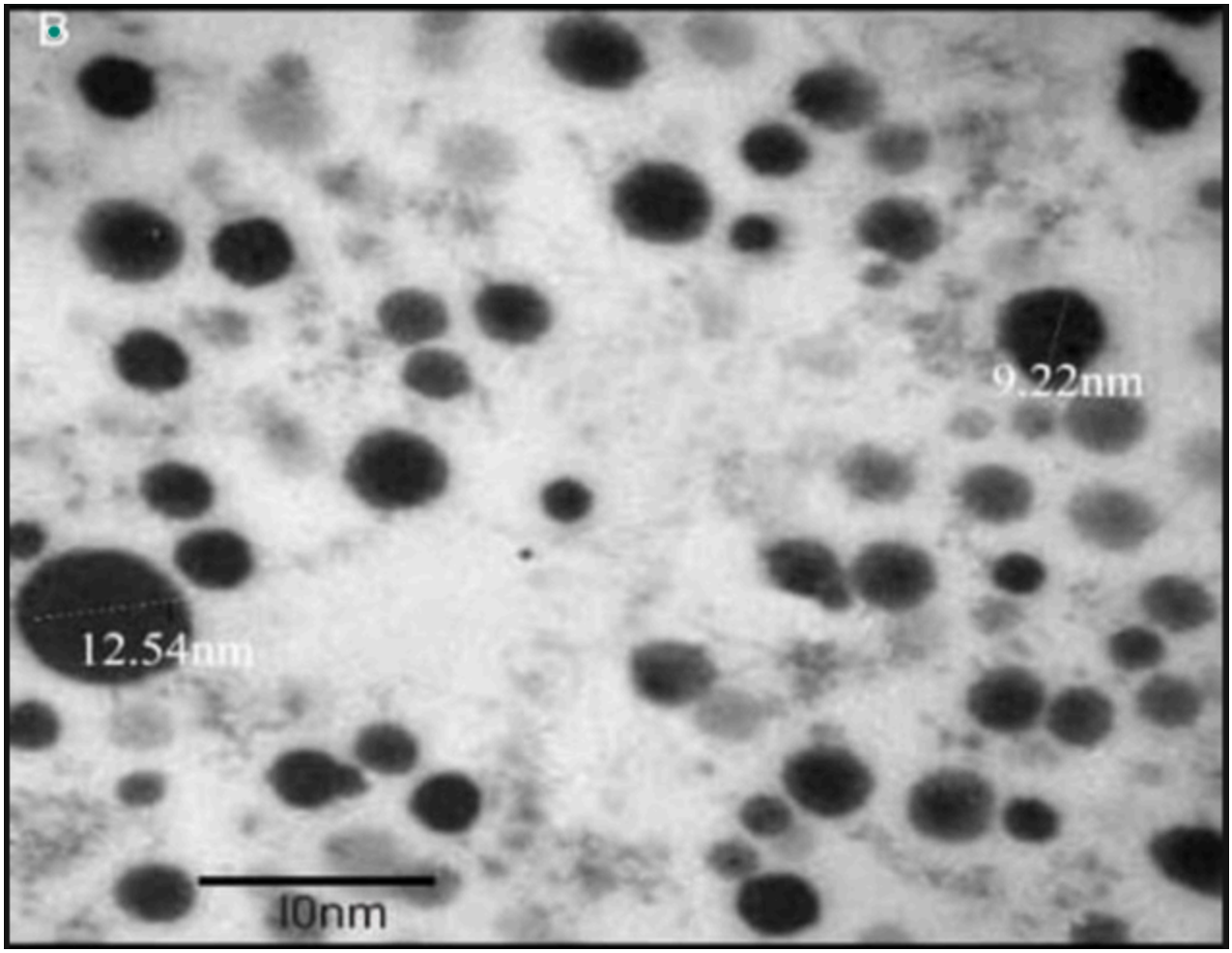

Figure 3

TEM micrograph of biosynthesised AgNPs showing predominantly spherical nanoparticles with mild local agglomeration. Two annotated particles have approximate diameters of 9.22 and 12.54 nm.

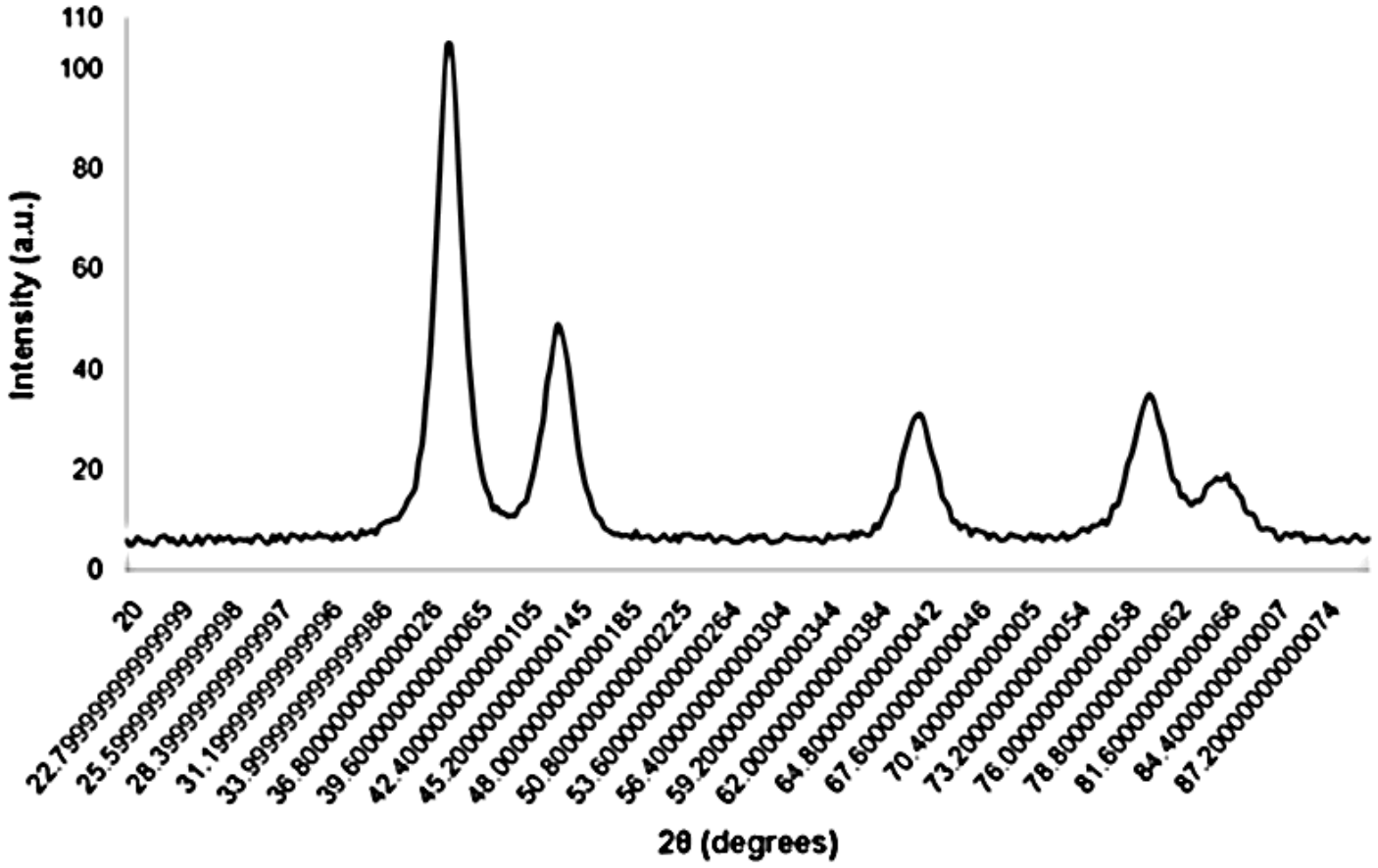

Figure 4

XRD pattern of biosynthesised AgNPs showing diffraction peaks indexed to the (111), (200), (220) and (311) crystallographic planes of face-centred cubic (fcc) silver. The average crystallite size calculated using the Debye–Scherrer equation was 16.5 ± 0.7 nm.

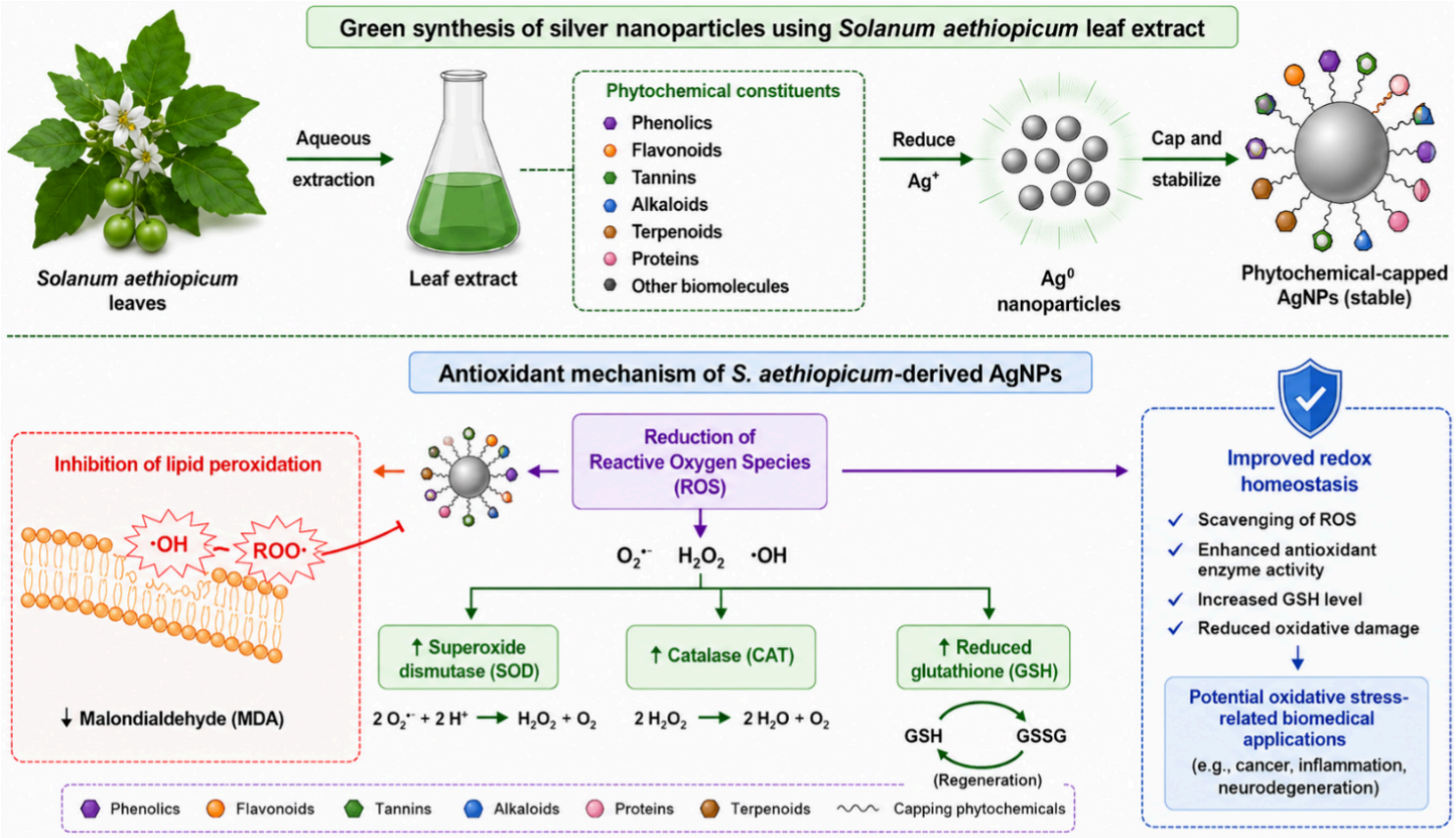

Figure 5

Proposed mechanism for the green synthesis and antioxidant activity of *Solanum aethiopicum*-derived silver nanoparticles. Phytochemicals including flavonoids, phenolics, tannins, and alkaloids reduce Ag^+ ions to Ag^0 nanoparticles and subsequently stabilise the nanoparticle surface. The proposed model links the phytochemical-capped AgNPs with inhibition of lipid peroxidation and the observed SOD, CAT and GSH assay responses. These pathways remain hypothetical pending validation in cellular and in vivo models.